Ligand Binding and the Catalytic Reaction of Cytochrome *caa*$_3$ from the Thermophilic Bacterium *Rhodothermus marinus*†

Håkan Sigurdson,‡ Andreas Namslauer,‡ Manuela M. Pereira,§ Miguel Teixeira,§ and Peter Brzezinski*,‡

Department of Biochemistry and Biophysics, The Arrhenius Laboratories for Natural Sciences, Stockholm University, SE-106 91 Stockholm, Sweden, and Instituto de Tecnologia Química e Biológica, Universidade Nova de Lisboa, Rua da Quinta Grande, 6, Apartado 127, 2780-156 Oeiras, Portugal

Received February 19, 2001; Revised Manuscript Received June 13, 2001

ABSTRACT: The ligand-binding dynamics and the reaction with O_2 of the fully (five-electron) reduced cytochrome *caa*$_3$ from the thermohalophilic bacterium *Rhodothermus* (*R.*) *marinus* were investigated. The enzyme is a proton pump which has all the residues of the proton-transfer pathways found in the mitochondrial-like enzymes conserved, except for one of the key elements of the D-pathway, the helix-VI glutamate [Glu(I-286), *R. sphaeroides* numbering]. In contrast to what has been suggested previously as general characteristics of thermophilic enzymes, during formation of the *R. marinus caa*$_3$−CO complex, CO binds weakly to Cu_B, and is rapidly ($k_{Ba} = 450\ s^{-1}$) trapped by irreversible ($K_{Ba} = 4.5 \times 10^3$) binding to heme a_3. Upon reaction of the fully reduced enzyme with O_2, four kinetic phases were resolved during the first 10 ms after initiation of the reaction. On the basis of a comparison to reactions observed with the bovine enzyme, these phases were attributed to the following transitions between intermediates (pH 7.8, 1 mM O_2): R → A ($\tau \cong 8\ \mu s$), A → P_r ($\tau \cong 35\ \mu s$), P_r → F ($\tau \cong 240\ \mu s$), F → O ($\tau \cong 2.5$ ms), where the last two phases were associated with proton uptake from the bulk solution. Oxidation of heme *c* was observed only during the last two reaction steps. The slower transition times as compared to those observed with the bovine enzyme most likely reflect the replacement of Glu(I-286) of the helix-VI motif -XGHPEV- by a tyrosine in the *R. marinus* enzyme in the motif -YSHPXV-. The presence of an additional, fifth electron in the enzyme was reflected by two additional kinetic phases with time constants of ∼20 and ∼720 ms during which the fifth electron reequilibrated within the enzyme.

Terminal oxidases are found in nearly all aerobic organisms on Earth where they constitute the last components of the respiratory chains and transfer electrons to molecular oxygen. The enzymes are integral membrane proteins that have in common ligands, which bind a heme group and a copper ion forming a binuclear center[1] at which O_2 is bound and reduced to water. In most oxidases characterized to date, the protons needed for this reaction (substrate protons) are taken up specifically from one side (N-side) of the membrane. In addition, the heme−copper oxidases conserve part of the energy released in the O_2-reduction chemistry to pump protons across the membrane [for review, see (*1*, *2*)].

Rhodothermus marinus is a thermohalophilic bacterium which grows optimally at 65 °C. Its membrane-bound electron-transfer chain has been extensively studied in the past few years. In addition to the dehydrogenases, the chain contains a recently characterized complex III, which is a multiheme cytochrome (*3*), a high-potential iron−sulfur protein (HiPIP) as an electron carrier (*4*, *5*), and two terminal oxidases, a cytochrome *cbb*$_3$ (*3*) and a cytochrome *caa*$_3$ (*6*).

The *R. marinus* cytochrome *caa*$_3$ has three redox-active cofactors in subunit I: heme *a*, and the binuclear center consisting of heme a_3 and Cu_B. In addition, subunit II contains two cofactors: Cu_A and a redox-active C-type heme (*3*, *7*). Thus, in contrast to many well-characterized terminal oxidases, the *R. marinus* enzyme has a total of five redox-active metal sites. Cytochrome *caa*$_3$ uses the HiPIP as an electron donor and transfers the electrons to molecular oxygen, which is reduced to water. In addition, it has recently been demonstrated that the enzyme pumps protons across the membrane with a stoichiometry of ∼1 H^+/e^- (*6*, *8*).

In other members of the oxidase family, two proton-conducting pathways (the D- and K-pathways) have been characterized in detail and shown to transfer pumped protons from solution toward the output side of the enzymes and substrate protons from solution to the binuclear center [for review, see (*9*)]. A comparison of the primary structure of subunit I from the *R. marinus* cytochrome *caa*$_3$ with the three-dimensional structures of cytochrome *c* oxidases from *Paracoccus denitrificans* and bovine heart shows that all residues found to be important in the D- and K-pathways

† These studies were supported by grants from The Swedish Foundation for International Cooperation in Research and Higher Education (STINT) and The Swedish Natural Science Research Council (to P.B.), and by FCT-Portugal Grant 36560/99 (to M.T.). M.M.P. is recipient of PRAXIS XXI Grant BPD/22054/99.

* Corresponding author. Fax: (+46)-8-153679; E-mail: peterb@dbb.su.se.

‡ Stockholm University.

§ Universidade Nova de Lisboa.

[1] Abbreviations: WT, wild type; Cu_A, copper A; Cu_B, copper B; τ, time constant [$\exp(-t/\tau)$]; binuclear center, heme a_3 and Cu_B; R, the fully reduced binuclear center; A, the fully reduced binuclear center with O_2 bound to Fe_{a3}; P_r, the peroxy intermediate formed at the binuclear center upon reaction of fully reduced cytochrome *c* oxidase with O_2 ($Fe_{a_3}^{4+}{=}O^{2-}$, $Cu_B^{2+}{-}OH^-$); F, oxo-ferryl intermediate; O, fully oxidized binuclear center.

10.1021/bi010344h CCC: $20.00
Published on Web 08/08/2001

are conserved, with the exception of a glutamate [Glu(I-286), *Rhodobacter sphaeroides* numbering] (*6*, *7*). This residue has been shown to play a key role in proton transfer through the D-pathway in other oxidases [see, e.g., (*10*)]. Homology-modeling studies of the *R. marinus* enzyme showed that a tyrosine residue [Tyr(I-256), *R. marinus* numbering] could structurally replace the glutamate. In the model, the phenol group of this residue is very close to the spatial position of the carboxyl group of the glutamate residue in the *P. denitrificans* and the bovine enzymes (*6*, *7*). Thus, the tyrosine may be a functional substitute of the glutamate residue in the proton pathway. A serine residue [Ser(I-257), *R. marinus* numbering], consecutive in sequence to the tyrosine and positioned in the model between Y(I-256) and the binuclear center, may also be involved in proton transfer. A comparison of the sequence of the *R. marinus* cytochrome caa_3 to those of other terminal oxidases has shown that this YS motif, in a helix-VI amino acid stretch, -YSHPXV- substituting for -XGHPEV- in the mitochondrial-like enzymes, is common to several other terminal oxidases (*6*, *7*).

In this study, we have investigated the kinetics of the reaction steps during oxidation of the fully reduced *R. marinus* cytochrome caa_3 by molecular oxygen using the flow-flash technique. The kinetics of proton uptake/release from/to the bulk solution were studied using pH-sensitive dyes. Internal electron-transfer reactions and proton-coupled electron transfer in the absence of oxygen were investigated after flash photolysis of CO from the mixed-valence enzyme in which heme a_3/Cu_B are reduced and hemes *a* and *c*, and Cu_A are oxidized [see (*11*)]. In addition, the dynamics of the ligand-binding pocket were studied by investigation of the kinetics of CO recombination after flash photolysis of the ligand from the fully reduced enzyme. The results are compared to those obtained with the mitochondrial-type enzymes and with enzymes from other thermophilic prokaryotes.

MATERIALS AND METHODS

Protein Purification. *Rhodothermus marinus* was grown and cytochrome caa_3 was purified as described in (*3*, *6*).

Recombination of the Fully Reduced-CO Complex at Different Solution CO Concentrations. The sample solution was transferred into a locally designed pressure cell in which the CO gas pressure over the sample surface can be varied. The enzyme was reduced by addition of 200 μM dithionite. The reactions after pulsed illumination of the sample were followed spectrophotometrically at 445 nm. Measurements were made at various CO pressures in the range 0.1−4 MPa, and the amount of dissolved CO in the solution was calculated using Henry's law.

Preparation of Two-Electron-Reduced (*Mixed-Valence*) *CO Complex*. The oxidized enzyme was transferred to a modified anaerobic cuvette. The atmosphere in the cuvette was exchanged by repetitive evacuation on a vacuum line and flushing with N_2. Finally, N_2 was replaced by CO. The incubation with CO results in formation of the mixed-valence CO complex (*12*) with heme a_3/Cu_B reduced and heme *a*/Cu_A/heme *c* oxidized. The reduction level was determined from the optical absorption spectrum and by inspection of flash-induced electron transfer after flash photolysis of CO [see (*13*)]. In cases where reduction of heme *a* was observed, the mixed-valence state was restored by titration with ferricyanide.

Preparation of the Fully Reduced-CO Complex. The buffer concentration in the enzyme stock solution was reduced to <10 μM by repetitive dilution with 100 mM KCl, 0.05% dodecyl-β-D-maltoside at pH 7.5 and reconcentration using a 50K-centrifuge filter (Millipore, Bedford, MA). The sample was then placed in a modified anaerobic cuvette. After addition of 5 μM PMS (phenazine methosulfate), the cuvette was repetitively evacuated on a vacuum line and flushed with N_2. To reduce the sample, 2 mM sodium ascorbate was added, followed by replacement of N_2 by CO.

Reaction of the Fully Reduced Enzyme with O_2. The kinetics of electron and proton transfer during reaction of fully reduced *R. marinus* enzyme with O_2 were studied using the flow-flash technique. The fully reduced-CO complex was mixed with an O_2-saturated buffer solution (see figure legends) at a ratio of 1:5. Carbon monoxide was flashed off in about 100 ms after mixing using a 10 ns, ∼50 mJ laser flash at 532 nm. Absorbance changes associated with the reaction were followed spectrophotometrically at various wavelengths. In the proton-uptake measurements, the mixing buffer in the flow-flash apparatus was replaced by a solution of 100 mM KCl, 0.05% dodecyl-β-D-maltoside, and phenol red at 48 μM. The exhaust from the flow-flash apparatus was collected in an anaerobic cuvette flushed with N_2 for buffer capacity calibration with HCl [see (*14*)].

Thermal CO Dissociation from the Fully Reduced Enzyme. The CO-dissociation kinetics (monitored at 430 nm) were measured by mixing the fully reduced-CO complex with an O_2-saturated buffer solution in a stopped-flow apparatus. The reaction of the fully reduced enzyme with O_2 is irreversible and rate-limited by the dissociation of CO.

RESULTS

Flash Photolysis of CO from the Fully Reduced Enzyme. Figure 1A shows the absorbance changes at 445 nm after pulsed illumination of the fully reduced enzyme−CO complex at 1 mM CO. After the increase in absorbance (at $t = 0$), attributed to CO-dissociation, there is a decrease with rate constants of $k'_{obs} \cong 26\,000\ s^{-1}$ and $k_{obs} \cong 100\ s^{-1}$. The faster component is attributed to transient binding of CO to Cu_B after dissociation from heme a_3 while the slower component is attributed to CO recombination to reduced heme a_3 (see Discussion). The same CO-recombination kinetics were observed in the pH range 6.5−8.5.

The rates of the two components were determined at different solution CO concentrations ranging from 1 to 40 mM (Figure 1B,C). Both rates increased with increasing CO concentration, but only the rate of the slower component (k_{obs}) saturated at high CO concentrations (Figure 1B). The relative contribution of the faster component to the observed absorbance changes decreased with increasing CO concentration (Figure 1D).

Thermal CO Dissociation from the Fully Reduced Enzyme. The CO-dissociation kinetics from heme a_3 were measured by mixing the fully reduced-CO complex with an O_2-saturated buffer solution in a stopped-flow apparatus. Since the CO ligand obstructs binding of O_2 to heme a_3, the irreversible reaction of the fully reduced enzyme with O_2 is

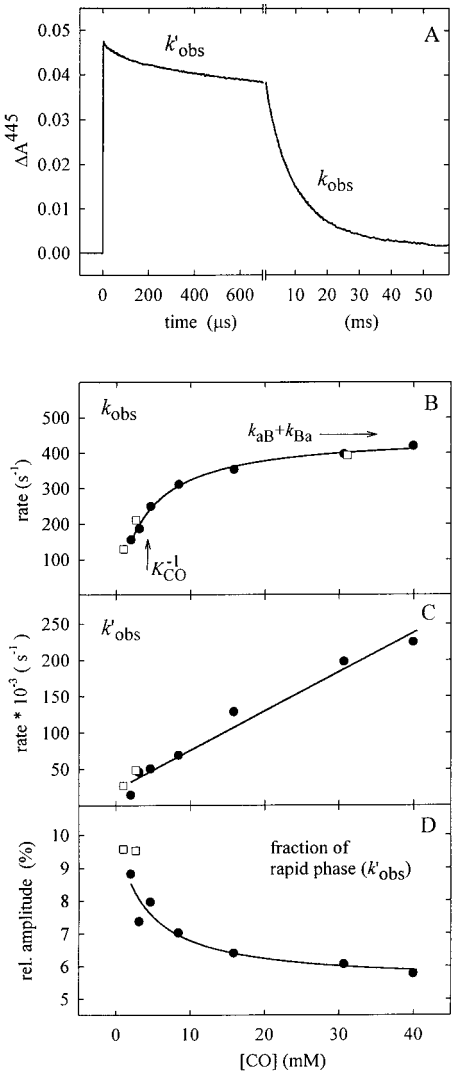

FIGURE 1: (A) Absorbance changes at 445 nm after pulsed illumination of the fully reduced-CO complex. The increase in absorbance is associated with CO dissociation. The following decrease is biphasic with two observed rate constants (k'_{obs} and k_{obs}) as shown in the graph. Experimental conditions: 100 mM Hepes−KOH, pH 7.5, 0.05% dodecyl-β-D-maltoside, 2 μM cytochrome *caa*$_3$ (~1 μM reacting enzyme), 200 μM sodium dithionite, 1 mM CO, 22 ± 1 °C. (B, C) Observed rates of CO-recombination (k_{obs}) and the fast phase (k'_{obs}) as a function of the bulk CO concentration. (D) Relative contribution of the amplitude of the rapid phase (k'_{obs}) to the sum of amplitudes of the two phases (k'_{obs} and k_{obs}). In B−D, the CO concentration was varied in the sample solution by applying an increasing pressure of CO over the sample surface in a pressure chamber. Measurements were first done at the lower CO concentrations, and the pressure was then increased during the experiment (●). To ensure that the gas and liquid phases were at equilibrium during the measurements, when the highest pressure was reached, it was then decreased, and two additional measurements were performed at the lower pressures (□). The solid lines are fits of the data to eqs 1−3 (see Discussion) and the parameter values are given in Table 2.

rate-limited by the thermal CO dissociation [see, e.g., (*15*)]. The reaction was monitored spectrophotometrically at 430 nm where a biphasic change in absorbance was observed (Figure 2). Complex oxidation kinetics have been observed previously (*15*), and the faster of the two components was taken to be associated with dissociation of CO from heme a_3, assuming that after mixing with O_2 no reaction can take place before dissociation of CO. The experiment was

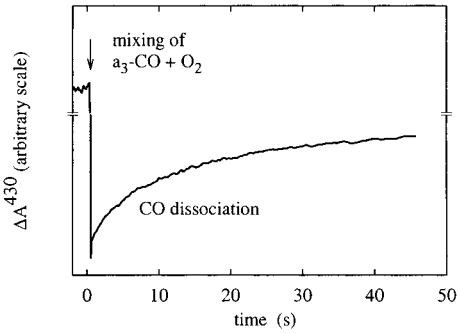

FIGURE 2: Absorbance changes monitored at 430 nm upon mixing the fully reduced CO complex and an O_2-saturated buffer solution in a stopped-flow apparatus (at $t = 0$). Since the CO ligand obstructs binding of O_2 to heme a_3, the irreversible reaction of the fully reduced enzyme with O_2 is limited by the CO-dissociation rate. A biphasic change in absorbance was observed. The faster of the two components was taken to be associated with dissociation of CO from heme a_3. Experimental conditions: 100 mM Hepes, pH 7.8, 0.05% dodecyl-β-D-maltoside, 22 ± 1 °C, 3.5 μM enzyme, 0.3 mM sodium ascorbate, 0.2 mM CO, 1 mM O_2.

repeated at different measuring-light intensities because the measuring light itself can dissociate CO from the complex, thus increasing the dissociation rate. Extrapolation of the rate to zero measuring-light intensity gave a CO dissociation rate of ~0.1 s^{-1} (not shown).

Internal Electron Transfer in the Absence of O$_2$. A mixed-valence-CO complex (reduced binuclear center and oxidized Cu_A, heme *a*, and heme *c*) was prepared. The CO ligand increases the apparent midpoint potential of heme a_3, stabilizing its reduced state. Figure 3 shows absorbance changes at 445 nm after flash photolysis of CO (increase in absorbance at $t = 0$). After the rapid increase in absorbance, associated with CO-dissociation from heme a_3, there is a fast decrease in absorbance that can be resolved into two phases (Figure 3A) with pH-independent (in the range 6.5−8.5) time constants of ~3 μs (3.3×10^5 s^{-1}) and ~22 μs (4.5×10^4 s^{-1}), respectively. The 3 μs phase is attributed to a fractional electron transfer from heme a_3 to heme *a* as a result of a lowered apparent redox potential of heme a_3 after CO dissociation. Assuming the same heme *a* and a_3 absorption coefficients (reduced minus oxidized states) for the *R. marinus* as for the bovine enzymes, about 25% of heme *a* was reduced during the 3 μs phase. The following 22 μs phase is attributed to a fractional electron transfer from the heme a_3/heme *a* equilibrium to Cu_A. No absorbance changes were observed at 550 nm; i.e., heme *c* was not reduced after flash photolysis of CO. The time constants for both electron-transfer reactions are in good agreement with those in the *R. sphaeroides* and bovine heart cytochrome *c* oxidases (*13*) (see Figure 3A). The CO-recombination kinetics were biphasic. The time constant of the faster phase ($\tau \cong 50$ ms) was pH-independent (not shown), and it was followed by a slower phase with a pH-dependent time constant of ~250 ms (~20% contribution) at pH 6.5 and ~1.5 s (~40% contribution) at pH 8.5 (Figure 3B).

Proton-Coupled Electron Transfer after CO Dissociation. In the bovine and *R. sphaeroides* enzymes at high pH (>7) is observed a slower, additional electron transfer from the binuclear center to heme *a*, coupled to proton release to the bulk solution. The same kinetic phase was observed also with the *R. marinus* cytochrome *caa*$_3$ (Figure 3C). The reaction was monitored at 598 nm, which is an isosbestic wavelength

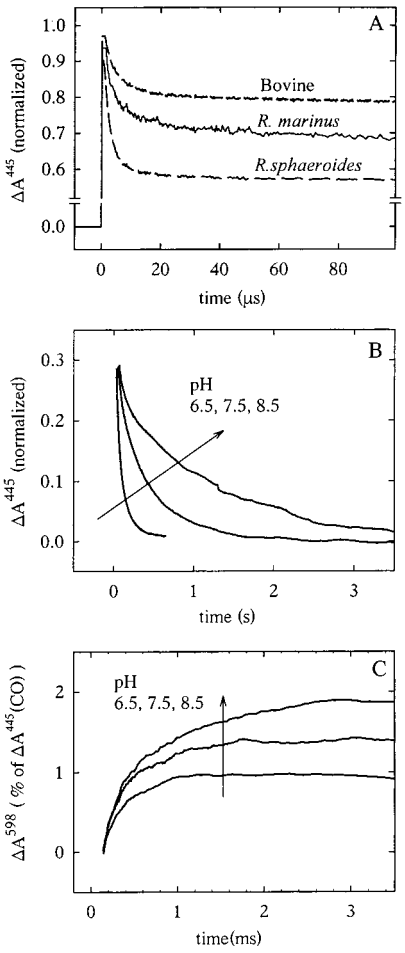

FIGURE 3: Absorbance changes at 445 nm (A, B) and 598 nm (C) after pulsed illumination of the mixed-valence enzyme−CO complex. For comparison, in (A) data obtained with the bovine and *R. sphaeroides* cytochrome aa_3 are shown (normalized to the CO-dissociation change). (B) Absorbance changes associated with CO recombination. The kinetics were biphasic where the time constant of the faster phase was ∼50 ms, independent of pH (6.5−8.5). The graph shows only the slower, pH-dependent component. The absorbance changes are normalized to the CO-dissociation changes at $t = 0$. (C) The absorbance changes at 598 nm are given as a percent of the CO-dissociation absorbance changes (at $t = 0$) at 445 nm. Experimental conditions: ∼1 μM enzyme, 200 mM Hepes, pH 7.5, 0.05% dodecyl-β-D-maltoside, 22 ± 1 °C.

for CO recombination and where the absorbance increase is mainly due to reduction of heme *a*. The time constant of the proton-coupled electron transfer was ∼0.42 ms (2400 s^{-1}) at pH 7.5.

Reaction of the Fully Reduced Enzyme with O_2. Figure 4 shows the time course of absorbance changes monitored at a number of wavelengths during reaction of fully reduced cytochrome caa_3 with O_2. The wavelengths are specific to transitions between oxygen intermediates and redox changes of the metal cofactors. In analogy with the reaction in the well-characterized enzymes from *R. sphaeroides* and bovine heart, the oxidative part of the reaction cycle of the caa_3 enzyme from *R. marinus* is assumed to follow the reaction steps as outlined below. The time constants and amplitudes of the transitions were determined from a global fit to a sum of four exponential functions from the traces monitored at 422 (not shown), 445, 550, 580, 590 (not shown), 605, and 830 nm in the time range of 0−9 ms (Table 1). In addition, to follow the time course of protonation changes, absorbance

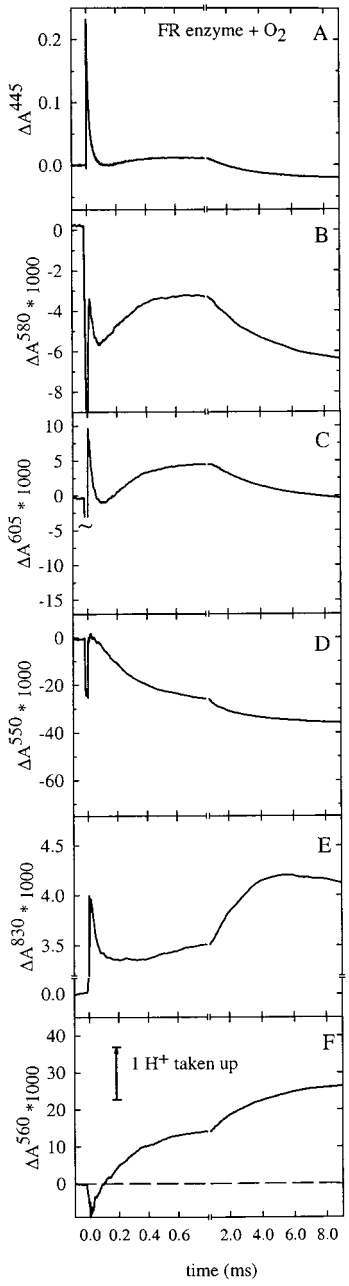

FIGURE 4: Absorbance changes associated with the reaction of fully reduced enzyme with O_2 followed spectrophotometrically at 445 nm (A), 580 nm (B), 605 nm (C), 550 nm (D), 830 nm (E), and 560 nm (F) (pH dye phenol red). The fully reduced-CO complex was mixed with an O_2-saturated solution at a ratio 1:5 about 100 ms before flash photolysis of CO (at $t = 0$). Conditions after mixing: 100 mM Tris, pH 7.8, 0.05% dodecyl-β-D-maltoside, 0.8 μM PMS (phenazine methosulfate), 0.3 mM sodium ascorbate, 1 mM O_2, 0.2 mM CO, 22 ± 1 °C, 3 μM enzyme. In (F), buffer was replaced by 100 mM KCl, and phenol red at 40 μM was added. The trace in (F) is the difference between traces obtained from measurement in an unbuffered and a buffered solution.

changes of the pH dye phenol red were monitored at 560 nm in the absence of buffer.

At 445 nm (Figure 4A), the increase in absorbance at $t = 0$, associated with CO dissociation, is followed by a kinetic phase attributed to binding of O_2 to reduced heme a_3 forming the A intermediate (R → A transition, $\tau \cong 8$ μs). The following phase ($\tau \cong 35$ μs) is associated with formation of the peroxy (P_r) intermediate, concomitant with oxidation of heme *a* as seen from the decrease in absorbance at 605 nm

Table 1: Rate Constants of Electron and Proton Transfer during Reaction of the Fully Reduced *R. marinus* (pH 7.8, 1 mM O_2) and *R. sphaeroides* Enzymes with O_2

reaction	*R. marinus* rate $\times 10^{-3}$ (s^{-1})	*R. sphaeroides*[a] rate $\times 10^{-3}$ (s^{-1})
R→A	120[b]	120[b]
A→P_r	28	18
P_r→F	4.2	7.4
F→O	0.4	0.75

[a] Values are from (*14*). After oxidation of the fully reduced *R. sphaeroides* cytochrome aa_3, also a slower kinetic phase with a rate of ~200 s^{-1} was observed (associated with proton uptake from the bulk solution). This phase is not included in the table. [b] This rate constant was fixed when fitting the other rate constants.

(Figure 4C). The transition was also monitored at 590 nm (not shown) where the signs of the R → A and A → P_r transitions are different, which facilitates the resolution of the A → P_r transition.

During formation of the next intermediate (oxo-ferryl, F, $\tau \cong 240$ μs), seen as an increase in absorbance at 580 nm (Figure 4B), there is a proton uptake from the bulk solution (Figure 4F). A simultaneous reduction of heme *a* is observed as an increase in absorbance at 605 nm. The absorbance decrease at 550 nm (Figure 4D) is associated with ~45% oxidation of heme *c*. It should be noted that there were no absorbance changes at 550 nm with time constants corresponding to the R → A or A → P_r transitions, indicating that heme *c* remains reduced until the P_r → F transition. At 830 nm, a wavelength characteristic of changes in the redox state of Cu_A (Figure 4E), there is a lag during the P_r → F transition, which is interpreted as an electron equilibration between heme *c*, Cu_A, and heme *a* that keeps Cu_A in the reduced state (see Discussion). In the last reaction step, the O intermediate is formed ($\tau \cong 2.5$ ms), associated with oxidation of heme *a* (absorbance decrease at 605 nm), heme *c* (absorbance decrease at 550 nm), and Cu_A (absorbance increase at 830 nm). Also in this step there is a proton uptake from the bulk solution (Figure 4F).

An additional kinetic phase with a time constant of ~20 ms followed that associated with the F → O transition. This phase was not observed with cytochrome aa_3 from *R. sphaeroides* nor from bovine heart, and it is presumably associated with redistribution of the fifth electron among the redox centers of the *R. marinus* enzyme.

DISCUSSION

We have investigated the dynamic characteristics of the catalytic site of cytochrome caa_3 from *Rhodothermus marinus*, and intramolecular electron and proton transfer during reaction of the fully reduced (five electrons) enzyme with oxygen.

Flash-Induced CO Dissociation and Recombination. The kinetics and thermodynamics of CO binding to the binuclear center have previously been used as a model for binding of O_2 and to investigate the structural and dynamic properties of the catalytic site [e.g., (*16*, *17*)]. In mitochondrial cytochrome *c* oxidase, after flash-induced dissociation of CO from heme a_3, the ligand binds transiently to Cu_B, followed by dissociation to the bulk solution with a time constant of ~1 μs (*18*, *19*). The following equation (eq 1) has been proposed to model the CO-dissociation/recombination process (*18*, *19*), where the transient binding of CO to Cu_B during recombination of the complex is reflected in saturating kinetics at high CO concentrations:

$$\underset{\text{FeCu}}{Fe_{a_3}^{2+}Cu_B^{+}} + CO \underset{k_{off}}{\overset{k_{on}}{\rightleftharpoons}} \underset{\text{FeCu(CO)}}{Fe_{a3}^{2+}Cu_B^{+}(CO)} \overset{k_{Ba}}{\underset{k_{aB}}{\rightleftharpoons}} \underset{\text{Fe(CO)Cu}}{Fe_{a3}^{2+}(CO)Cu_B^{+}} \quad (1)$$

where the two equilibrium constants are defined as $K_{CO} = k_{on}/k_{off}$ and $K_{Ba} = k_{Ba}/k_{aB}$.

Also with the *R. marinus* enzyme the CO-recombination kinetics saturated at high CO concentrations (see Figure 1B), which indicates that the model above (eq 1) also applies to this enzyme. The CO dissociation rate (k_{aB}) in the dark was determined to be ~0.1 s^{-1}. Assuming $[CO]k_{on}$, $k_{off} \gg k_{Ba}$, k_{aB} and [CO] ≫ [enzyme] (see below and Table 2), the observed CO-recombination rate (k_{obs}) can be described by [see also (*20*)]:

$$k_{obs} = k_{aB} + k_{Ba}\frac{k_{on}[CO]}{k_{off} + k_{on}[CO]} = k_{aB} + k_{Ba}\frac{[CO]}{K_{CO}^{-1} + [CO]} = k_{aB} + k_{Ba}\alpha \quad (2)$$

where α is the fraction of CO bound to Cu_B^+ during the recombination process. Thus, at saturating CO concentrations, i.e., $[CO] \gg K_{CO}^{-1}$, $\alpha \cong 1$ and $k_{obs} \cong k_{aB} + k_{Ba}$. The graph in Figure 1B shows that k_{obs} saturates at ~450 s^{-1}, and since $k_{aB} \cong 0.1$ s^{-1}, $k_{Ba} \cong k_{obs} \cong 450$ s^{-1}. The two rate constants k_{on} and k_{off} cannot be determined individually from the data in Figure 1B, but their ratio, K_{CO}^{-1}, corresponds to the CO concentration at which k_{obs} equals half of the maximum rate, i.e., $K_{CO}^{-1} \cong 4$ mM.

Pulsed illumination of the enzyme−CO complex [state Fe(CO)Cu] results in essentially an infinite k_{aB} during ~10 ns (i.e., the duration of the laser flash), forming state FeCu(CO), followed by dissociation to the bulk solution. With the bovine enzyme, the release of CO from Cu_B is detected indirectly as an absorbance change in a wavelength range in which heme a_3 absorbs (*19*). For example, at 445 nm, a decay in absorbance is observed after flash-induced CO dissociation from heme a_3. Therefore, we attribute the rapid decay (k'_{obs}) with a rate constant of ~26 000 s^{-1} at 1 mM CO (Figure 1A) to transient binding of CO to Cu_B. The rate of the rapid absorbance decay at 445 nm increased with increasing CO concentration (Figure 1C), and the amplitude decreased as shown in Figure 1D, which is consistent with the model in eq 1. Assuming that the absorbance change is due to decay of state FeCu(CO), the amplitude is (assuming $k_{on}[CO]$, $k_{off} \gg k_{Ba}$, k_{aB}; see above)

$$\Delta A \propto \frac{k_{off}}{k_{off} + [CO]k_{on}} \quad (3)$$

The model predicts that this absorbance change vanishes at high CO concentrations. However, the absorbance change itself most likely reflects also a relaxation in the heme pocket that controls dissociation of CO from Cu_B [see (*19*)]. This relaxation is expected to take place also at high CO

Table 2: Comparison of Kinetic and Thermodynamic Parameters for CO Binding to the Binuclear Center (See Equation 1 and Figure 5) of Bovine (*19*), *R. sphaeroides* (*20*), and *A. ambivalens* (*20*) Cytochrome *aa*$_3$, *T. thermophilus* Cytochrome *ba*$_3$ (*21*), and *R. marinus* Cytochrome *caa*$_3$ (This Work)

constant	bovine	*R. sphaeroides*	*A. ambivalens*	*T. thermophilus*	*R. marinus*
k_{aB} (s^{-1})	0.027	0.01	1.2	0.8	0.1
k_{Ba} (s^{-1})	1030	750	1.9	8	450
K_{Ba}	3.8×10^4	7.5×10^4	1.6	10	4.5×10^3
k_{off} (s^{-1})	7.9×10^5	−	1.4×10^4	−	2.2×10^4
k_{on} ($M^{-1} s^{-1}$)	6.8×10^7	−	$\sim 10^9$	−	5.4×10^6
K_{CO}^{-1} (mM)	11	16	$\sim 1.3 \times 10^{-2}$	$<10^{-1}$	4

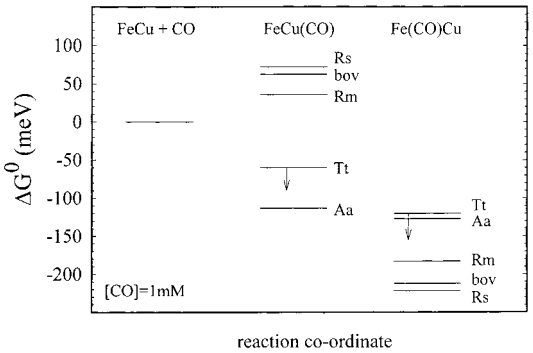

FIGURE 5: Energy diagram showing the energetics of CO recombination of the fully reduced enzymes with CO. The different states and equilibrium constants are defined in eq 1, and their values are summarized in Table 2. Energy levels are given for a CO concentration of 1 mM. The arrow at Tt indicates that an upper limit of the free energy was given in (*21*). Enzymes are the following: Rs, cyt *aa*$_3$ from *R. sphaeroides*; bov, cyt *aa*$_3$ from bovine heart; Rm, cyt *caa*$_3$ from *R. marinus*; Tt, cyt *ba*$_3$ from *T. thermophilus*; Aa, cyt *aa*$_3$ from *A. ambivalens*. With the Rs, bov, and Rm enzymes, binding of CO to Cu_B is endergonic, and the ligand is then trapped at heme a_3 by a highly exergonic transfer of CO. With the Tt and Aa enzymes, CO binding to Cu_B is exergonic, followed by equilibration with heme a_3.

concentrations, which is the reason we observe an absorbance change also at the high CO concentrations. The observed rate of CO dissociation from Cu_B after flash photolysis of the enzyme−CO complex is the sum of rates k_{on}[CO] and k_{off}. A fit of the model in eq 1 with the data in Figure 1C gives $k_{off} \cong 22\,000\ s^{-1}$.

For the bovine-heart enzyme, the CO-recombination reaction is characterized by a relatively large K_{CO}^{-1}, i.e., a small affinity of CO for Cu_B^+ ($\alpha = 0.08$ at 1 mM CO) (*17*−*19*). The relatively rapid ligand binding to heme a_3 is maintained by a large k_{Ba} of $\sim 10^3\ s^{-1}$. In the reduced enzyme−CO complex, in the dark, a very small fraction of CO is bound to Cu_B^+ because k_{Ba} ($\sim 10^3\ s^{-1}$) $\gg k_{aB}$ ($\sim 0.027\ s^{-1}$). Qualitatively, the same behavior was observed for the *R. sphaeroides* cytochrome *c* oxidase (*20*) (see Table 2). However, a different situation was found with the *Acidianus* (*A.*) *ambivalens* (*20*) and *Thermus* (*T.*) *thermophilus* (*17*, *21*) oxidases (Table 2, Figure 5). For example, for the *A. ambivalens* quinol oxidase, K_{CO}^{-1} is small; i.e., the affinity of CO for Cu_B^+ is large ($\alpha \cong 1$ at 1 mM CO) and k_{Ba} is $\sim 1.9\ s^{-1}$, i.e., much smaller than with the mitochondrial enzyme. In addition, in the reduced enzyme−CO complex, in the dark, a large fraction of CO is bound to Cu_B^+ because k_{Ba} ($1.9\ s^{-1}$) $\cong k_{aB}$ ($1.1\ s^{-1}$).

In conclusion, with the mitochondrial-type enzymes, the CO affinity for Cu_B^+ is small, but the transfer rate from Cu_B to heme a_3 is large, while the opposite is observed for the enzymes from the thermophiles from *A. ambivalens* and *T. thermophilus* that grow at temperatures >75 °C (see Figure 5). It has been proposed that the high affinity for the ligand in the thermophilic enzymes reflects an adaptation to the low oxygen-concentration environments in which the bacteria grow [see, e.g., (*21*)]. *R. marinus* is a moderate thermophile, with an optimum growth temperature of 65 °C, that thrives in a narrow habitat close to marine hot springs where it finds a delicate balance between the optimal growth temperature and the oxygen concentration needed to aerobic growth. However, although being a strict aerobe and thermophile, ligand binding to the cytochrome *caa*$_3$ enzyme displays characteristics more similar to those of the mitochondrial-like enzymes ($\alpha = 0.2$ at 1 mM CO, i.e., a relatively low affinity for CO; see Table 2 and Figure 5) than to those of the other thermophilic oxidases. Thus, the previously proposed postulate is not general, and may simply reflect a variability of the properties of heme−copper oxidases.

Internal Electron Transfer in the Absence of CO. Several of the partial reaction steps during reaction of the fully reduced enzyme with O_2 involve internal electron-transfer reactions. Therefore, before discussing specific steps of the reaction of the fully reduced enzyme with O_2 and proton-coupled electron transfer, we note that the observed rates for the electron transfer between hemes *a* and a_3 and between heme *a* and Cu_A were $\sim 3.3 \times 10^5\ s^{-1}$ (sum of the forward and backward rates) and $\sim 4.5 \times 10^4\ s^{-1}$, respectively, i.e., similar to those observed with the *R. sphaeroides* and bovine enzymes (*13*).

Proton-Coupled Electron Transfer in the Absence of O$_2$. The rapid, internal electron transfer after CO dissociation from the mixed-valence enzyme is followed by a slower, additional electron transfer from the binuclear center to heme *a*. In the bovine and *R. sphaeroides* enzymes, this electron transfer has been shown to be coupled to proton release to the bulk solution through the K-pathway [cf. (*9*)], where the proton donor most likely is a water molecule that after proton release binds as a hydroxide to heme a_3 or Cu_B [see (*9*, *11*)]. A corresponding kinetic phase was also observed with the *R. marinus* enzyme (Figure 3C). The hydroxide binding is presumably reflected in the biphasic CO-recombination kinetics, where the relative contribution of the slower component increased with increasing pH (Figure 3B). At pH 7.5, the slow phase of the CO-recombination displayed a rate of $\sim 2.2\ s^{-1}$, i.e., much slower than CO recombination with the fully reduced enzyme, even when considering that the fraction of reduced binuclear center during the recombination process is less than 100% [cf. (*13*, *22*)]. The slow component in the CO recombination most likely reflects the OH^- binding at the binuclear center, where the OH^- must dissociate before CO can bind.

Reaction of the Fully Reduced Enzyme with O_2. After dissociation of CO, initially O_2 binds to heme a_3 with a rate of 1.2×10^5 s^{-1} (at 1 mM O_2), forming intermediate A. It has been observed previously that with the bovine cytochrome *c* oxidase, O_2 binds transiently to Cu_B before binding to heme a_3, which suggests that CO should dissociate before O_2 can bind. With the *R. marinus* enzyme, the CO-dissociation rate from Cu_B (k_{off}) was estimated to be $\sim 2.2 \times 10^4$ s^{-1}, which indicates that O_2 can bind to heme a_3 before CO is released from Cu_B. A similar situation was observed previously with the ubiquinol oxidase (cytochrome bo_3) from *E. coli* in which heme CO dissociates from Cu_B with a rate constant of $\sim 10^3$ s^{-1} (*16*, *23*) while in the flow-flash experiment O_2 binds to the reduced heme o_3 with a rate of $\sim 10^5$ s^{-1} at 1 mM O_2 [*24*−*26*; see also discussion in (*16*)]. As suggested previously (*27*), it is possible that the two ligands bind independently, but the O−O bond cannot be cleaved (during formation of P_r) until CO dissociates from Cu_B because the breaking of the O−O bond involves binding of OH^- to Cu_B. This scenario is consistent with the results observed with the *R. marinus* cytochrome caa_3, where the release of CO from Cu_B ($\tau \cong 48$ μs) and formation of P_r ($\tau \cong 35$ μs) display similar time constants.

The F intermediate was formed with a time constant of 240 μs, most clearly seen as an increase in absorbance at 580 nm (Figure 4B). This $P_r \rightarrow F$ rate is about a factor of 2 slower than with the *R. sphaeroides* or bovine enzymes. In the *R. sphaeroides* cytochrome *c* oxidase, the transition was shown to be rate-limited by intramolecular proton transfer from E(I-286) to the binuclear center (*28*, *29*), followed by rapid reprotonation of E(I-286) from the bulk solution. Thus, the slower $P_r \rightarrow F$ rate in the *R. marinus* enzyme is consistent with a different composition of protonatable groups/water molecules in the D-pathways of the two enzymes (see below). In the *R. sphaeroides* and bovine enzymes, this reaction step is also associated with rereduction of heme *a* by Cu_A. In the *R. marinus* enzyme, the situation is more complicated as Cu_A is in rapid equilibrium with the bound heme *c* [see also (*30*, *31*)]. This is why there is essentially no net oxidation of Cu_A (no change in absorbance at 830 nm on the time scale of F formation), and a decrease in absorbance is seen at 550 nm, associated with oxidation of heme *c*. The heme *a* reduction and proton uptake from the bulk solution during $P_r \rightarrow F$ are detected as an increase in absorbance at 605/445 and 560 nm, respectively.

In the following $F \rightarrow O$ transition, a fourth electron is transferred to the binuclear center from the heme *c*/Cu_A/heme *a* equilibrium with a time constant of 2.5 ms, which results in a decrease in absorbance at 445 and 605 nm (oxidation of heme *a* and decay of F) and at 550 nm (oxidation of heme *c*), and an increase in absorbance at 830 nm (oxidation of Cu_A) and at 560 nm (proton uptake from the bulk solution). Also this reaction is about a factor of 2 slower than with the *R. sphaeroides* or bovine enzymes. The "final" absorbance levels in Figure 4 are not the same as those observed with, for example, the *R. sphaeroides* enzyme because after completition of the $F \rightarrow O$ transition in the *R. marinus* enzyme there is a fifth electron within the enzyme. As indicated from the elevated absorbance levels at 445, 550,and 605 nm, this electron is most likely distributed within the heme *c*/Cu_A/heme *a* equilibrium.

On a much slower time scale ($\tau \cong 20$ ms), we observed further absorbance changes, presumably associated with a redistribution of the fifth electron among the redox centers and possibly also among different enzyme molecules.

In the *R. marinus* cytochrome caa_3, the $P_r \rightarrow F$ and $F \rightarrow O$ transitions were associated with proton uptake from the bulk solution, as observed previously with the bovine and *R. sphaeroides* cytochrome *c* oxidases (*14*). In the *R. sphaeroides* enzyme, both pumped and substrate protons are taken up through the D-pathway during oxygen reduction [see (*9*)]. Thus, the transfer of the two "types of protons" must be controlled by the enzyme so that the substrate protons are not transferred to the binuclear center before pumped protons are taken up. It was suggested that E(I-286) may play the role of such a control element by switching between two different positions in which the side chain can provide protonic contact with the binuclear center and the output side of the protein, respectively (*32*, *33*).

In *R. marinus* cytochrome caa_3, E(I-286) is not conserved. Nevertheless, the enzyme pumps protons across the membrane (*8*). A structural model of subunit I from the *R. marinus* cytochrome caa_3 shows that the hydroxyl group of a helix-VI tyrosine residue [Tyr(I-256), *R. marinus* numbering] is found near the spatial position corresponding to that of the carboxylate group of E(I-286) (*3*, *7*). A consecutive serine residue [Ser(I-257), *R. marinus* numbering] may also be part of the proton pathway. Also cytochrome caa_3 from *Thermus thermophilus*, which has the same substitution pattern in helix-VI as that of the *R. marinus* cytochrome caa_3 (*34*, *35*), is a proton pump. Thus, assuming that the pumping mechanism is the same in all oxidases, the pumping machinery is presumably not found around E(I-286), but rather elsewhere in the enzyme.

A more drastic example is the aa_3 quinol oxidase from *Acidianus ambivalens*, which is a fully efficient proton pump (Gomes et al., submitted for publication) without having any of the residues forming the canonical D- and K-pathways (*36*). Analysis of a 3D model for this enzyme led to the suggestion that a glutamate residue in helix-II could be the functional substitute of E(I-286) (*27*, *37*). This conclusion is also supported by the observation that even though the replacement of E(I-286) by Gln or Ala in *R. sphaeroides* cytochrome *c* oxidase results in an inactive enzyme, partial activity as well as proton pumping can be restored by placing another glutamate on the opposite side of the D-pathway with the side chain at about the same location as that of the native E(I-286) (*38*). Moreover, recent experiments showed that in the *P. denitrificans* cytochrome *c* oxidase, E(I-286) can be replaced by an arrangement of amino acid residues which resembles that found in the *R. marinus* cytochrome caa_3, resulting in enzyme that pumps protons (*39*). The presence of a Tyr rather than a Glu in the *R. marinus* enzyme (either in helix-VI, as in the mitochondrial-like enzymes, or in helix-II, as in *A. ambivalens* cytochrome aa_3) may be reflected in the slower $P_r \rightarrow F$ and $F \rightarrow O$ transition rates in the *R. marinus* than in, e.g., the *R. sphaeroides* enzyme (at the same pH) (*14*, *27*). Taken together, the results indicate that a chain of water molecules and protonatable/hydrophilic residues is important for the transfer of substrate and pumped protons through the D-pathway, but this chain has been arranged in different ways throughout evolution.

ACKNOWLEDGMENT

We thank Pia Ädelroth for experimental assistance.

REFERENCES

1. Ferguson-Miller, S., and Babcock, G. T. (1996) *Chem. Rev. 96*, 2889−2907.
2. Zaslavsky, D., and Gennis, R. B. (2000) *Biochim. Biophys. Acta 1458*, 164−179.
3. Pereira, M. M., Carita, J. N., and Teixeira, M. (1999) *Biochemistry 38*, 1268−1275.
4. Pereira, M. M., Antunes, A. M., Nunes, O. C., Dacosta, M. S., and Teixeira, M. (1994) *FEBS Lett. 352*, 327−330.
5. Pereira, M. M., Carita, J. N., and Teixeira, M. (1999) *Biochemistry 38*, 1276−1283.
6. Pereira, M. M., Santana, M., Soares, C. M., Mendes, J., Carita, J. N., Fernandes, A. S., Saraste, M., Carrondo, M. A., and Teixeira, M. (1999) *Biochim. Biophys. Acta 1413*, 1−13.
7. Santana, M., Pereira, M. M., Elias, N. P., Soares, C. M., and Teixeira, M. (2001) *J. Bacteriol. 183*, 687−699.
8. Pereira, M. M., Verkhovskaya, M. L., Teixeira, M., and Verkhovsky, M. I. (2000) *Biochemistry 39*, 6336−6340.
9. Brzezinski, P., and Ädelroth, P. (1998) *J. Bioenerg. Biomembr. 30*, 99−107.
10. Ädelroth, P., Karpefors, M., Gilderson, G., Tomson, F. L., Gennis, R. B., and Brzezinski, P. (2000) *Biochim. Biophys. Acta 1459*, 533−539.
11. Ädelroth, P., Sigurdson, H., Hallén, S., and Brzezinski, P. (1996) *Proc. Natl. Acad. Sci. U.S.A. 93*, 12292−12297.
12. Brzezinski, P., and Malmström, B. G. (1985) *FEBS Lett. 187*, 111−114.
13. Ädelroth, P., Brzezinski, P., and Malmström, B. G. (1995) *Biochemistry 34*, 2844−2849.
14. Ädelroth, P., Ek, M., and Brzezinski, P. (1998) *Biochim. Biophys. Acta 1367*, 107−117.
15. Antonini, G., Brunori, M., Malatesta, F., Sarti, P., and Wilson, M. T. (1987) *J. Biol. Chem. 262*, 10077−10079.
16. Varotsis, C., Kreszowski, D. H., and Babcock, G. T. (1996) *Biospectroscopy 2*, 331−338.
17. Woodruff, W. H. (1993) *J. Bioenerg. Biomembr. 25*, 177−188.
18. Woodruff, W. H., Einarsdóttir, Ó., Dyer, R. B., Bagley, K. A., Palmer, G., Atherton, S. J., Goldbeck, R. A., Dawes, T. D., and Kliger, D. S. (1991) *Proc. Natl. Acad. Sci. U.S.A. 88*, 2588−2592.
19. Einarsdóttir, Ó., Dyer, R. B., Lemon, D. D., Killough, P. M., Hubig, S. M., Atherton, S. J., Lopez-Garriga, J. J., Palmer, G., and Woodruff, W. H. (1993) *Biochemistry 32*, 12013−12024.
20. Aagaard, A., Gilderson, G., Gomes, C. M., Teixeira, M., and Brzezinski, P. (1999) *Biochemistry 38*, 10032−10041.
21. Giuffrè, A., Forte, E., Antonini, G., D'Itri, E., Brunori, M., Soulimane, T., and Buse, G. (1999) *Biochemistry 38*, 1057−1065.
22. Verkhovsky, M. I., Morgan, J. E., and Wikström, M. (1992) *Biochemistry 31*, 11860−11863.
23. Lemon, D. D., Calhoun, M. W., Gennis, R. B., and Woodruff, W. H. (1993) *Biochemistry 32*, 11953−11956.
24. Verkhovsky, M. I., Morgan, J. E., Puustinen, A., and Wikström, M. (1996) *Biochemistry 35*, 16241−16246.
25. Hirota, S., Mogi, T., Ogura, T., Hirano, T., Anraku, Y., and Kitagawa, T. (1994) *FEBS Lett. 352*, 67−70.
26. Svensson-Ek, M., Thomas, J. W., Gennis, R. B., Nilsson, T., and Brzezinski, P. (1996) *Biochemistry 35*, 13673−13680.
27. Gilderson, G., Aagaard, A., Gomes, C., Ädelroth, P., Teixeira, M., and Brzezinski, P. (2001) *Biochim. Biophys. Acta 1503*, 261−270.
28. Smirnova, I. A., Ädelroth, P., Gennis, R. B., and Brzezinski, P. (1999) *Biochemistry 38*, 6826−6833.
29. Karpefors, M., Ädelroth, P., Aagaard, A., Smirnova, I. A., and Brzezinski, P. (1999) *Isr. J. Chem. 39*, 427−437.
30. Hill, B. C. (1994) *J. Biol. Chem. 269*, 2419−2425.
31. Giuffrè, A., D'Itri, E., Giannini, S., Brunori, M., Ubbink-Kok, T., Konings, W. N., and Antonini, G. (1996) *J. Biol. Chem. 271*, 13987−13992.
32. Riistama, S., Hummer, G., Puustinen, A., Dyer, R. B., Woodruff, W. H., and Wikström, M. (1997) *FEBS Lett. 414*, 275−280.
33. Iwata, S., Ostermeier, C., Ludwig, B., and Michel, H. (1995) *Nature 376*, 660−669.
34. Mather, M. W., Springer, P., Hensel, S., Buse, G., and Fee, J. A. (1993) *J. Biol. Chem. 268*, 5395−5408.
35. Hon-Nami, K., and Oshima, T. (1984) *Biochemistry 23*, 454−460.
36. Purschke, W. G., Schmidt, C. L., Petersen, A., and Schäfer, G. (1997) *J. Bacteriol. 179*, 1344−1353.
37. Gomes, C. M., Pereira, M. M., Santana, M., and Teixeira, M. (1999) *J. Inorg. Biochem. 74*, 311−311.
38. Aagaard, A., Gilderson, G., Mills, D. A., Ferguson-Miller, S., and Brzezinski, P. (2000) *Biochemistry 39*, 15847−15850.
39. Backgren, C., Hummer, G., Wikström, M., and Puustinen, A. (2000) *Biochemistry 39*, 7863−7867.

BI010344H